



HAL
open science

Characterization on thermal hysteresis of shape memory alloys via macroscopic interface propagation

Chengguan Zhang, Xue Chen, Olivier Hubert, Yongjun He

► To cite this version:

Chengguan Zhang, Xue Chen, Olivier Hubert, Yongjun He. Characterization on thermal hysteresis of shape memory alloys via macroscopic interface propagation. *Materialia*, 2024, 33, pp.102038. 10.1016/j.mtla.2024.102038 . hal-04733729

HAL Id: hal-04733729

<https://cnrs.hal.science/hal-04733729v1>

Submitted on 12 Oct 2024

HAL is a multi-disciplinary open access archive for the deposit and dissemination of scientific research documents, whether they are published or not. The documents may come from teaching and research institutions in France or abroad, or from public or private research centers.

L'archive ouverte pluridisciplinaire **HAL**, est destinée au dépôt et à la diffusion de documents scientifiques de niveau recherche, publiés ou non, émanant des établissements d'enseignement et de recherche français ou étrangers, des laboratoires publics ou privés.

Characterization on thermal hysteresis of shape memory alloys via macroscopic interface propagation

Chengguan Zhang ^a, Xue Chen ^b, Olivier Hubert ^c, Yongjun He ^{a, *}

^a*LMI, UME, ENSTA Paris, Institut Polytechnique de Paris, 91120 Palaiseau, France*

^b*Faculty of Engineering and Environment, Northumbria University, Newcastle Upon Tyne, UK*

^c*LMPS, Université Paris-Saclay, CentraleSupélec, ENS Paris-Saclay, CNRS, 91190 Gif-sur-Yvette, France.*

* Corresponding Author. Email address: yongjun.he@ensta-paris.fr (Y.J. He)

Abstract

An SMA specimen starts martensitic phase transformation normally by the nucleation of a macroscopic austenite-martensite interface at the specimen's boundary (i.e., the nucleation is sensitive to boundary conditions). By contrast, the interface propagation only needs to overcome the energy barrier of the incompatibility between the austenite and martensite phases (i.e., the interface-propagation driving force reflects material's intrinsic properties). In this paper, we observe the thermally induced forward and reverse *quasi-static* propagation of the macroscopic austenite-martensite interface in a Ni-Mn-Ga single-crystal bar. It is found that the temperature difference between the forward and reverse propagation is only 2.8 °C which is obviously less than the thermal hysteresis evaluated from Differential Scanning Calorimetry measurement (6.3 °C) on the same material. This result not only gives a better characterization of the thermal hysteresis of the phase transformation, but also helps deeply understand the relation between the phase-transformation kinetics and the microstructures of the macroscopic austenite-martensite interface.

Keywords: Temperature hysteresis, austenite-martensite interface, martensitic phase transformation, shape memory alloy, Ni-Mn-Ga single crystal.

1. Introduction

Hysteresis and interface are the two main features of the 1st order phase transformation (martensitic transition) in Shape Memory Alloys (SMAs) [1-3]. These two features are closely related to each other as shown in Fig.1(a) for a superelastic SMA bar under tension (quasi-static displacement-controlled loading-unloading): the forward and reverse martensitic phase transition occur via the nucleation and propagation of a macroscopic austenite-martensite interface (A-M interface), demonstrating the stress hysteresis which significantly influences the damping capability of SMA dampers [4-7] and the efficiency of SMA actuators [8]. It has been well accepted that the stress hysteresis is defined as the difference between the forward and reverse interface propagation stresses ($\sigma^H_{\text{Propagation}} \equiv \sigma^{\text{up}}_{\text{Propagation}} - \sigma^{\text{low}}_{\text{Propagation}}$) [9, 10], rather than that of the interface nucleation stresses ($\sigma^H_{\text{Nucleation}} \equiv \sigma^{\text{up}}_{\text{Nucleation}} - \sigma^{\text{low}}_{\text{Nucleation}}$) as shown in Fig. 1(a).

The characterization on the stress hysteresis via the macroscopic interface forward/reverse propagation in Fig. 1(a) is general for both polycrystalline and single-crystal SMAs [5, 11]. Indeed, the microstructures of the macroscopic interface can be very different in various SMAs. For example, the macroscopic interface in NiTi polycrystal has many partially-transformed grains (and each grain contains further low-scale microstructure) while the macroscopic interface of Ni-Mn-Ga single crystal contains laminates. But both the polycrystal and the single crystal share the same global physical picture: the macroscopic interface propagation triggers the material points (on and/or near the interface) to take the phase transformation with numerous microscopic (and/or meso-scale) instability events causing energy dissipation (hysteresis), which can be characterized by the plateau stresses. Compared to the stress hysteresis of the interface propagation, the characterization on the thermal hysteresis via observing macroscopic interface is rare in literature.

The temperature-induced phase transformation occurs via the macroscopic interface nucleation and propagation as reported in [12-15]. It is quite natural to estimate the thermal driving force for the phase transformation with the temperature at

1 the propagating interface [14, 16-18]. However, in literature, the most popular method
2 to characterize the thermal driving forces is DSC (Differential Scanning Calorimetry),
3 which usually gives four typical temperatures: martensite start/finish temperatures
4 M_s/M_f and austenite start/finish temperatures A_s/A_f . Unfortunately, those four
5 temperatures have no direct relation with the interface propagation. Moreover, there are
6 various definitions of thermal hysteresis T^H in literature [19], such as $T^H \equiv (A_f + A_s - M_f$
7 $- M_s)/2$ [20, 21], $T^H \equiv A_f - M_s$ [22, 23], and $T^H \equiv A_s - M_s$ [12].

8 To clarify these issues, in this paper, we perform both DSC test and the in-situ
9 temperature measurements of the thermally induced forward and reverse quasi-static
10 propagating austenite-martensite interface in Ni-Mn-Ga SMA single crystal. The main
11 results of the two methods are compared in Fig. 1(b) where the temperature hysteresis
12 of the forward and reverse propagating interface ($T^H_{\text{Propagation}}=2.8$ °C) is obviously
13 smaller than that of DSC measurement ($T^H_{\text{DSC}} \equiv \frac{A_s + A_f - M_s - M_f}{2} \approx 6.3$ °C). Further, our
14 measured temperature hysteresis of the propagating interface ($T^H_{\text{Propagation}}= 2.8$ °C) is
15 less than all the values of T^H_{DSC} reported in literature for various Ni-Mn-Ga SMAs as
16 summarized in Table 1. While the standard DSC measurement on our material is given
17 in Appendix, the in-situ temperature measurements of the thermally induced forward
18 and reverse quasi-static propagating austenite-martensite interface are detailed in the
19 following.

20 **2. Material and experimental procedures**

21 To perform the temperature measurement on the thermally induced quasi-static
22 interface propagation, we developed an experimental setup (Fig. 2(a)) with a
23 $\text{Ni}_{50}\text{Mn}_{28}\text{Ga}_{22}$ (at. %) single-crystal rectangular bar ($20 \times 2.5 \times 1$ mm³, from
24 Goodfellow) with all faces approximately along the $\{100\}$ planes of the parent cubic
25 austenite phase. Before the thermal loading, the specimen is in five-layered martensite
26 phase (5M) at room temperature (around 20 °C) as our DSC measurement on the
27 material shows $M_f= 33.7^\circ\text{C}$ in Fig. 1(b). On the other hand, the initial state of the whole
28 specimen can be set to be an approximately tetragonal single martensite variant by

1 mechanical compression along the z -direction (i.e, the direction along the specimen's
2 1mm thickness) [13, 24, 25]. Then, for a stress-free condition, the specimen was simply
3
4 put on two supports (a polymer one on the left and an aluminum one on the right, as
5
6 shown in Fig. 2(a)). The aluminum support can easily transfer the heat from the heater
7
8 to the specimen's end, where a thermocouple (K-Type of sheath diameter of 0.5 mm) is
9
10 adopted to record the thermal loading as shown in Fig. 2(a). By setting the heater's
11
12 temperature to increase stepwise and then decrease (the red dashed line in Fig 2(a)), the
13
14 temperature of the specimen's right end (the grey solid line in Fig 2(a)) slowly increases
15
16 (with a rate of $0.1^{\circ}\text{C}/\text{min}$) up to 53°C ($> A_f = 41.6^{\circ}\text{C}$) and then decreases to room
17
18 temperature. The thermal loading is so slow that the quasi-static macroscopic interface
19
20 propagation (just like stick-slip motion) can be achieved as shown in Figs. 2(b) and 2(c)
21
22 where the bar's top surface (x - y plane) is observed by an Infra-Red (IR) camera (FLIR
23
24 X8501SC). The bar's top surface is covered by a thin carbon layer (candle black) to
25
26 improve its IR emissivity. Due to the carbon-layer imperfection, the measuring error of
27
28 the surface is around $\pm 0.16^{\circ}\text{C}$.
29
30

31 **3. Results and discussions**

32
33
34
35 With the IR camera, the detailed temperature evolutions of the quasi-static
36
37 propagating interface during heating and cooling are recorded, respectively, into
38
39 Movies 1 and 2 (supplementary materials) whose typical frames and the associated
40
41 interface positions are shown in Figs. 2(b) and 2(c). It is noted that, from the interface
42
43 stick-slip motion in Fig. 2(b), we can identify the temperature for the start of the
44
45 interface slip motion (denoted as $T^{\text{slip-start}}$) based on the IR images of Fig. 2(c) for the
46
47 forward and reverse interface slip motions at the time instants t_i and the interface
48
49 positions x_i . The data of the IR images of Fig. 2(c) are two-dimensional temperature
50
51 distribution changing with time ($t_1 \sim t_{13}$). To facilitate observations and comments, we
52
53 plot the temperature profiles along the specimen's length direction (i.e., the temperature
54
55 distribution at the centre line of specimen's top surface along the x -direction in Fig. 2(a))
56
57 for the time instants $t_1 \sim t_{13}$ in Fig. 3. It is found that the slip-start temperature of the
58
59
60
61
62
63
64
65

1 heating-induced forward interface propagation ($t_1 \sim t_7$) is $T^{\text{slip-start}}_{\text{heating}}=37.7 \pm 0.2 \text{ }^\circ\text{C}$
2 while that of the cooling-induced reverse interface propagation ($t_8 \sim t_{13}$) is $T^{\text{slip-}}$
3 $\text{start}_{\text{cooling}}=34.9 \pm 0.2 \text{ }^\circ\text{C}$; their difference (around $2.8 \text{ }^\circ\text{C}$) can be considered as the thermal
4 hysteresis of the forward and reverse phase transformation. The uncertainty (0.2°C) is
5 close to the measurement error that is mainly caused by emissivity fluctuations and
6 small surface defects (as observed in each temperature profile in Fig. 3). On the other
7 hand, the magnified views in Fig. 4 of the detailed temperature evolutions of the
8 slipping processes (S1~S7 for heating-induced forward propagation and S8~S13 for
9 cooling-induced reverse propagation) give similar results: $T^{\text{slipping}}_{\text{heating}} = 37.7 \pm 0.3 \text{ }^\circ\text{C}$ for
10 the forward propagation while $T^{\text{slipping}}_{\text{cooling}} = 34.9 \pm 0.3 \text{ }^\circ\text{C}$ for the reverse propagation;
11 their difference is still around $2.8 \text{ }^\circ\text{C}$.
12
13
14
15
16
17
18
19
20
21
22

23 It is also seen in the global view of Fig. 4(a) that the slipping interface's temperature
24 is higher than the sticking interface's during heating-induced forward propagation. By
25 contrast, the global view of Fig. 4(b) shows that the slipping interface's temperature is
26 always lower than the sticking interface's during the cooling-induced reverse
27 propagation. That means, there is a temperature range around $2.8 \text{ }^\circ\text{C}$ ($T^{\text{slipping}}_{\text{heating}} >$
28 $T > T^{\text{slipping}}_{\text{cooling}}$) for the sticking interface (no interface motion), which implies
29 hysteretic behavior.
30
31
32
33
34
35
36

37 It should be noted that, in the current experiments, the small thermal gradient drives
38 the propagation of a single-interface. As shown in Fig. 3, the thermal gradient is not
39 large (around $0.6 \text{ }^\circ\text{C}/\text{mm}$ and $0.4 \text{ }^\circ\text{C}/\text{mm}$ for heating and cooling respectively). So, the
40 A-M interface velocities during the slipping process are less than $20 \text{ } \mu\text{m}/\text{s}$ (see the
41 magnified views in Fig. 4), which can be approximately considered as a quasi-static
42 interface propagation. It is also noted from the magnified views of Fig.4 that most of
43 the interface speeds during heating are higher than those during cooling. That might be
44 due to two factors: One is the slight difference in the thermal gradient between the
45 heating ($0.6 \text{ }^\circ\text{C}/\text{mm}$) and cooling ($0.4 \text{ }^\circ\text{C}/\text{mm}$); the other is the asymmetry in the heat
46 production during the forward/reverse martensitic phase transformation because the
47 dissipation always generates heat while the material needs to release/absorb latent heat
48
49
50
51
52
53
54
55
56
57
58
59
60
61
62
63
64
65

1 during the A→M (M→A) transformation.

2 Besides the thermal gradient loading, one might propose to use *homogeneous*
3 heating/cooling (uniformly increasing/decreasing the specimen's temperature) to drive
4 the phase transformation. But homogeneous loading would lead to the nucleation of
5 multiple interfaces and their simultaneous propagation. This complicated situation is
6 similar to the phase transformation of a superelastic SMA under stress-controlled
7 loading (snap through as shown in Fig. 1(a)) where interface nucleation/propagation
8 and the associated hysteresis are significantly different from the quasi-static case (see
9 details in [26-28]). As discussed in [5] for the superelastic SMA under tension, the
10 nucleation stresses ($\sigma^{\text{up}}_{\text{Nucleation}}$ and $\sigma^{\text{low}}_{\text{Nucleation}}$ in Fig. 1(a)) depend on the specimen's
11 shape and boundary conditions. Similarly, for thermally induced phase transformation
12 in SMA single crystal [15], the nucleation prefers to occur at specimen's boundary. So,
13 the nucleation process and the associated driving force would significantly depend on
14 the quality of the cutting edges of the specimen.
15
16
17
18
19
20
21
22
23
24
25
26
27
28

29 By contrast, the driving force for the interface propagation does not depend on
30 the boundary, but on the compatibility of the macroscopic austenite-martensite interface
31 whose microstructures observation and associated energy analysis have been reported
32 in [12, 13, 29-31]. In fact, the microstructures of the macroscopic interface are not
33 randomly formed, but quite regularly developed (e.g., laminates shown in the two
34 inserts of Fig. 3). According to [30] and [29], the interfacial microstructures are
35 governed by the energy minimization based on the material's fundamental parameters
36 (such as the atomic lattice mismatch between phases and variants). That means, the
37 thermal hysteresis caused by the interfacial energy barrier in fact is related to the
38 material's fundamental parameters. Moreover, the energy dissipation density
39 (hysteresis) is widely adopted as an important material parameter in material
40 constitutive models in literature, such as [32] and [33].
41
42
43
44
45
46
47
48
49
50
51
52
53

54 The compatibility only depends on the lattice parameters of the two phases
55 (austenite and martensite), which means that the driving force (temperature hysteresis)
56 associated with the interface propagation can be considered as a material's intrinsic
57
58
59
60

property.

To provide good compatibility between the austenite and martensite phases in order to achieve small hysteresis (low energy dissipation), some research groups have fabricated other SMAs such as $Zn_{45}Au_xCu_{55-x}$ ($20 < x < 30$) [34] and $TiNiX$, ($X = Cu, Pt, Pd, Au$) [1], trying to tune the lattice parameters to satisfy the compatibility criterion, so-called “middle eigenvalue λ_2 equal to 1” or “cofactor condition” [1, 35]. The typical value of the “extremely small temperature hysteresis” is about 2.045 °C, which was measured by DSC in [34]. According to our current study (Fig. 1(b)), DSC measurement obviously over-estimates the real hysteresis (the interface-propagation temperature hysteresis). Therefore, a single-crystal SMA bar of the “extremely small hysteresis” would probably exhibit an interface-propagation temperature hysteresis much less than 2 °C. That means, the interface propagation of such optimal SMA would be very near a thermodynamically reversible process (with little energy dissipation).

Moreover, the austenite-martensite interface of the optimal SMA with “extremely small hysteresis” is very special: an interface separating the austenite and a single martensite variant (without martensite twinning), so-called twinless A-M interface. Such interface is very sharp (consisting of only several atomic layers) and its thickness is smaller than nanometer as observed by the high-resolution electron microscopy (TEM) in [21]. By contrast, our material (Ni-Mn-Ga) in current study has a diffuse A-M interface (with the interfacial zone of the thickness around 1 μ m) consisting of various martensite twinning laminates as observed in our previous experiments [12, 13, 36]. According to the interfacial energy analysis [29-31], the twinning A-M interface would have much larger interface energy (energy barrier of phase transformation) than the twinless A-M interface of the optimal SMA of the “extremely small hysteresis”. The relation between the interfacial energy (barrier) and the hysteresis (energy dissipation) has been well studied [1, 2, 37]: the higher the interfacial barrier, the larger hysteresis (energy dissipation) is needed for the phase transformation. In other words, the driving force (hysteresis) of the diffuse interface should be much larger than that of the atomically sharp interface of the optimal SMA. Now the hysteresis of our diffuse

1 interface is 2.8°C. So, the optimal SMA's sharp interface propagation hysteresis should
2 be much less than that value.
3

4 The current study also implies that, if the phase transformation occurs only via
5 interface propagation (i.e., without interface nucleation), the energy dissipation
6 (hysteresis) of SMA actuators or other SMA-based devices would be more efficient or
7 more sensitive. For example, the interface in the specimen of the current study can have
8 cyclic forward and reverse propagations without reaching the specimen's ends under
9 proper thermal loadings.
10

11 Before ending the discussion, we can also briefly comment on other methods in
12 literature for characterizing the thermal hysteresis, such as by measuring the
13 temperature dependence of electric resistance and magnetization[22, 38-42], where the
14 temperature is controlled to monotonically increase and then monotonically decrease,
15 which is just like the stress-controlled loading triggering the snap-through in Fig. 1. So,
16 those measured thermal hysteresis would not be the same as the interface-propagation
17 temperature hysteresis reported here. Moreover, some of those methods might not be
18 consistent with the DSC measurement. For example, the authors of the reference[22]
19 searching for low-hysteresis SMAs reported that the thermal hysteresis measured by
20 the electric resistance was near zero (less than 1°C) while their DSC measurements
21 indicated a much larger hysteresis ($T_{DSC}^H = \frac{A_s + A_f - M_s - M_f}{2}$ was larger than 10 °C). Further,
22 their resistance measurement showed $M_s \gg A_s$ (see the inset in Fig. 1 of [22]) while
23 their DSC results showed $M_s \leq A_s$ (see the inset in Fig. 6(d) of [22]). That means, for
24 the different methods, there are no consistent definitions of the phase transformation
25 temperatures and the associated hysteresis, which poses obstacles in the future research
26 when comparing and utilizing the material's phase-transformation properties reported
27 in the literature.
28
29
30
31
32
33
34
35
36
37
38
39
40
41
42
43
44
45
46
47
48
49
50
51
52

53 A better characterization of the thermal hysteresis would help to deeply understand
54 the relation between phase transformation kinetics and the microstructures of the
55 macroscopic austenite-martensite interface, and provide hints for searching for low-
56
57
58
59
60
61
62
63
64
65

1 hysteresis materials and associated engineering applications.
2
3

4 **4. Conclusions**

5
6 In summary, the thermal hysteresis measured by the temperature difference (2.8 °C)
7 between the forward and reverse quasi-static interface propagation is obviously less
8 than that of the DSC measurement (6.3 °C), which usually includes the nucleation of
9 multiple interfaces. By contrast with the boundary-dependent nucleation, the interface
10 propagation is preferable to indicate the material's intrinsic hysteretic behavior, because
11 its energy dissipation is governed by the interfacial incompatibility caused by the
12 different lattice parameters of the austenite and martensite phases. The current study
13 also implies that SMA actuators or other SMA-based devices would be more efficient
14 or more sensitive if phase transformation occurs only via interface propagation (i.e.,
15 without interface nucleation).
16
17
18
19
20
21
22
23
24
25
26
27
28
29
30
31
32
33
34
35
36
37
38
39
40
41
42
43
44
45
46
47
48
49
50
51
52
53
54
55
56
57
58
59
60
61
62
63
64
65

Table 1 DSC measurement on thermal hysteresis of various Ni-Mn-Ga SMAs in literature

| Content (at. %) | | | | | | | | | Thermal hysteresis (°C) | Ref. |
|-----------------|------|------|------|-------|-------|-------|-------|---------------|--|------|
| Alloy | Ni | Mn | Ga | M_s | M_f | A_s | A_f | Phase | $T_{DSC}^H \equiv \frac{A_s + A_f - M_s - M_f}{2}$ | |
| 1 | 50 | 28 | 22 | 38.6 | 36.3 | 44.8 | 46.8 | 5M | 8.35 | [43] |
| 2 | 50 | 28 | 22 | 36.5 | 35.5 | 41.5 | 42.2 | 5M | 5.85 | [25] |
| 3 | 50 | 28.8 | 21.2 | 50 | 49 | 58 | 60 | 5M | 9.5 | [44] |
| 4 | 52 | 23 | 25 | 35 | 31 | 41 | 45 | Not mentioned | 10 | [38] |
| 5 | 50.7 | 28.4 | 20.9 | 61 | 52 | 66 | 72 | 5M | 12.5 | [45] |
| 6 | 50.7 | 28.3 | 21 | 57 | 50 | 65 | 70 | 5M | 14 | |
| 7 | 50.7 | 27.8 | 21.5 | 52 | 50 | 58 | 61 | 5M | 8.5 | |
| 8 | 50.6 | 28.5 | 20.9 | 60 | 58 | 66 | 68 | 5M | 8 | |
| 9 | 50 | 29.8 | 20.2 | 71 | 67 | 74 | 78 | 5M | 7 | |
| 10 | 50 | 28.9 | 21.1 | 48 | 38 | 47 | 57 | 5M | 9 | |
| 11 | 49.9 | 29.9 | 20.2 | 71 | 65 | 77 | 81 | 5M | 11 | |
| 12 | 49.7 | 29.1 | 21.2 | 38 | 36 | 46 | 48 | 5M | 10 | |
| 13 | 49.6 | 29.2 | 21.2 | 30 | 28 | 36 | 36 | 5M | 7 | |
| 14 | 49.2 | 30.6 | 20.2 | 55 | 50 | 60 | 64 | 5M | 9.5 | |
| 15 | 49.1 | 30.7 | 20.2 | 51 | 48 | 59 | 62 | 5M | 11 | |
| 16 | 49 | 30.3 | 20.7 | 39 | 36 | 45 | 50 | 5M | 10 | |
| 17 | 48.5 | 30.3 | 21.2 | 29 | 26 | 32 | 35 | 5M | 6 | |
| 18 | 51 | 28.5 | 20.5 | 83 | 77 | 81 | 87 | 7M | 4 | |
| 19 | 50.5 | 29.4 | 20.1 | 78 | 70 | 75 | 84 | 7M | 5.5 | |
| 20 | 49.5 | 30.3 | 20.2 | 68 | 64 | 71 | 75 | 7M | 7 | |
| 21 | 48.8 | 31.4 | 19.8 | 64 | 60 | 65 | 69 | 7M | 5 | |
| 22 | 54.9 | 23.8 | 21.3 | 286 | 268 | 295 | 314 | NM | 27.5 | |
| 23 | 54 | 24.7 | 21.3 | 224 | 214 | 225 | 237 | NM | 12 | |
| 24 | 53.9 | 24.4 | 21.7 | 257 | 251 | 278 | 287 | NM | 28.5 | |
| 25 | 53.7 | 26.4 | 19.9 | 250 | 239 | 265 | 273 | NM | 24.5 | |
| 26 | 53.3 | 24.6 | 22.1 | 192 | 186 | 195 | 203 | NM | 10 | |
| 27 | 52.9 | 25 | 22.1 | 75 | 71 | 81 | 90 | NM | 12.5 | |
| 28 | 52.8 | 25.7 | 21.5 | 117 | 94 | 104 | 131 | NM | 12 | |
| 29 | 52.7 | 26 | 21.3 | 161 | 143 | 151 | 173 | NM | 10 | |
| 30 | 52.4 | 25.6 | 22 | 150 | 141 | 151 | 161 | NM | 10.5 | |
| 31 | 52.3 | 27.4 | 20.3 | 125 | 118 | 130 | 135 | NM | 11 | |
| 32 | 51.7 | 27.7 | 20.6 | 110 | 96 | 108 | 121 | NM | 11.5 | |
| 33 | 51.5 | 26.8 | 21.7 | 120 | 101 | 107 | 127 | NM | 6.5 | |
| 34 | 51.2 | 27.4 | 21.4 | 98 | 93 | 98 | 102 | NM | 4.5 | |
| 35 | 51 | 28.7 | 20.3 | 106 | 93 | 103 | 112 | NM | 8 | |

| | | | | | | | | | |
|----|------|------|------|-----|-----|-----|-----|----|-----|
| 36 | 50.5 | 30.4 | 19.1 | 118 | 103 | 110 | 124 | NM | 6.5 |
| 37 | 47 | 33.1 | 19.9 | 53 | 50 | 56 | 58 | NM | 5.5 |

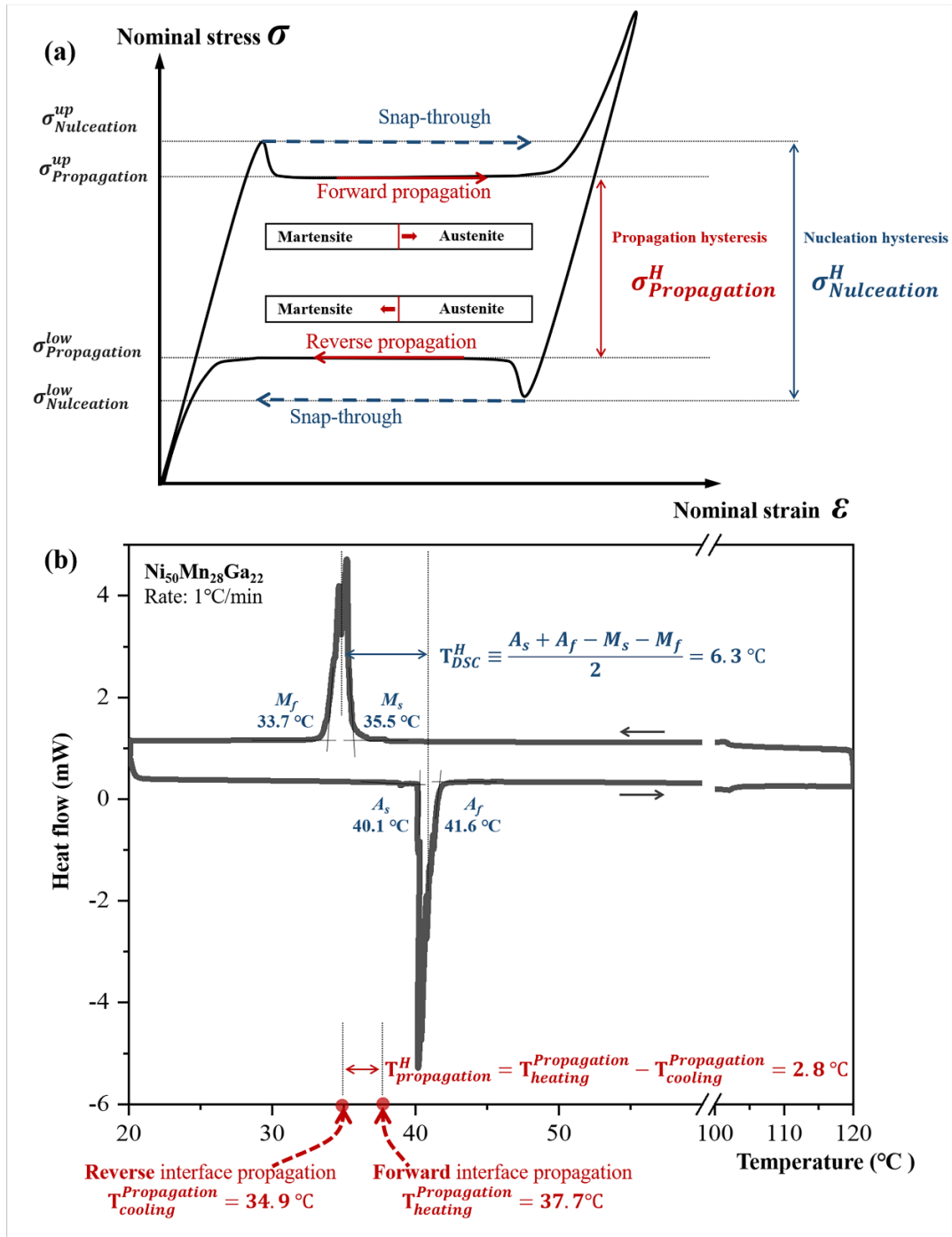


Figure 1: (a) Typical loading-unloading stress-strain curve of the austenite-martensite interface propagation in superelastic SMA under tension. (b) Comparison of thermal hysteresis of the DSC test and the temperature hysteresis of the quasi-static forward and reverse interface propagation.

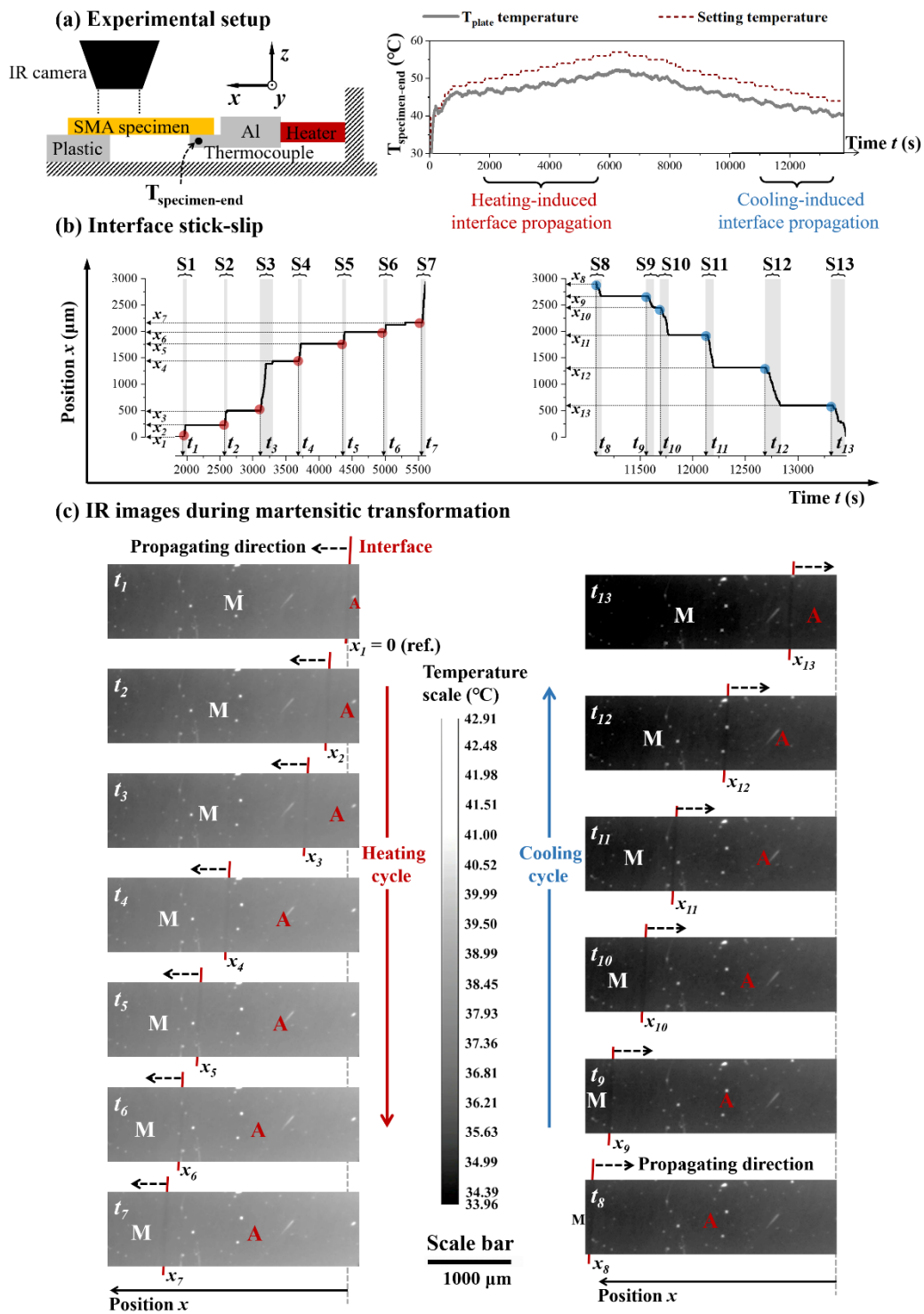


Figure 2: (a) The experimental setup and the slow thermal loading (gradual temperature increase and decrease at the specimen's right end); (b) Position of the single interface changes with time during the heating-induced forward propagation and the cooling-induced reverse propagation (analyzed from Movies 1 and 2 in the supplementary materials); (c) Typical IR images at different time instants $t_1 \sim t_{13}$ of the Movies 1 and 2.

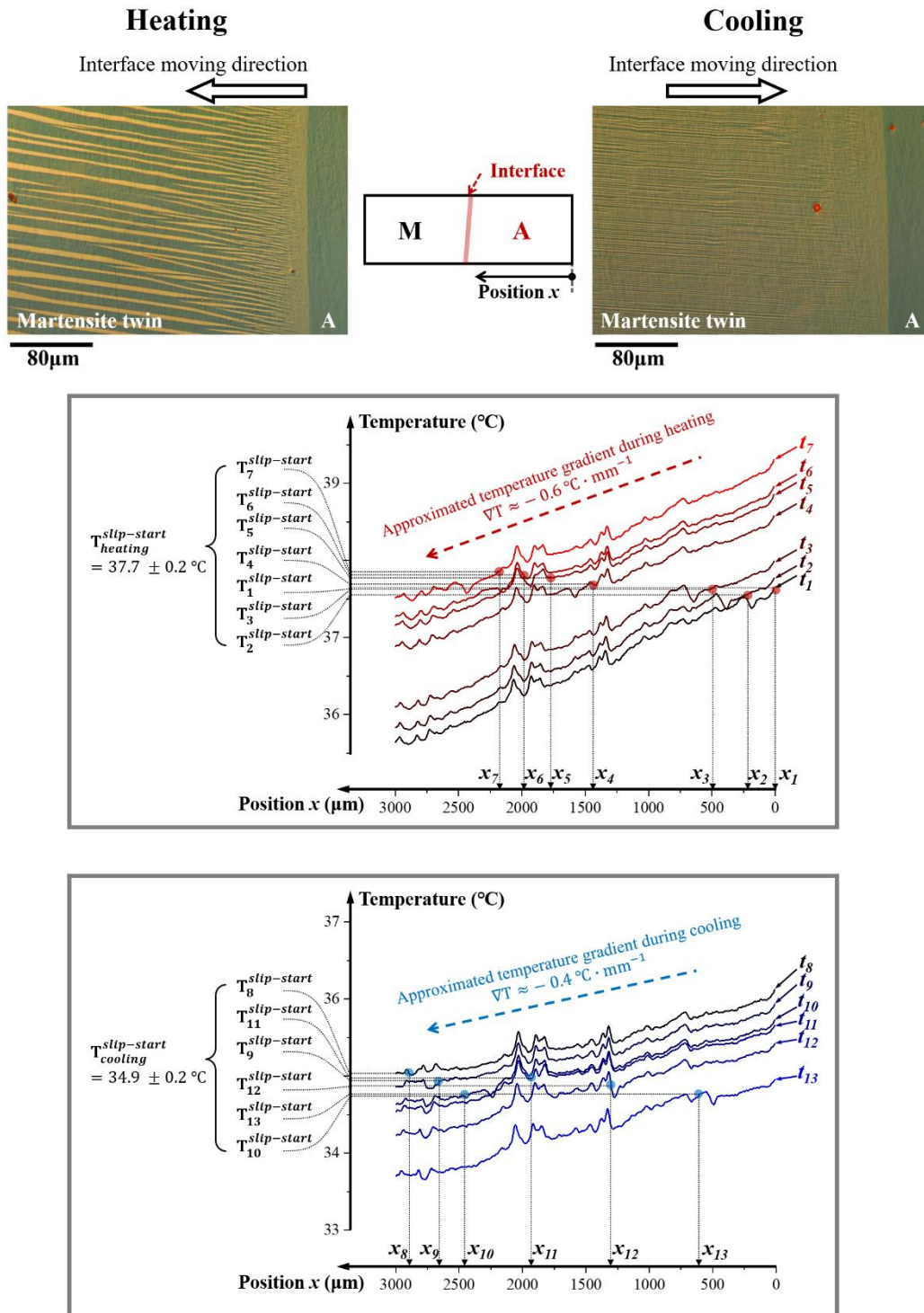


Figure 3 Temperature profiles along the specimen's length direction (x -axis) at time instants $t_1 \sim t_{13}$ are combined with the interface's positions to determine the temperatures at the start of the interface slipping motions during heating and cooling (The two inserts are the microstructures of the macroscopic interface during heating and cooling respectively, which are similar to the observation in [12]).

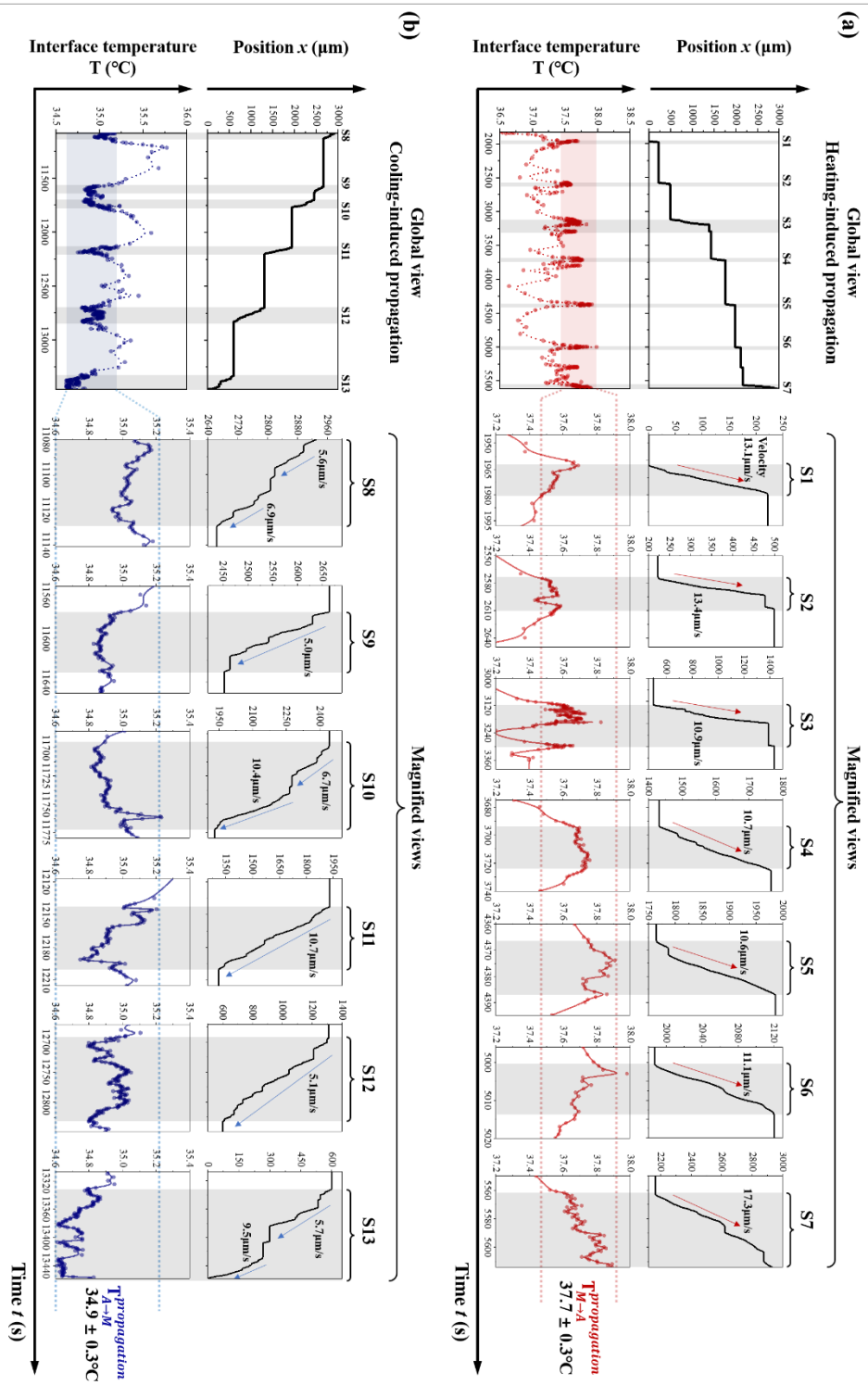


Figure 4: Global view show the temperature variations in both interface sticking and slipping processes while the magnified views show the detailed temperature variation during the slipping processes and the associated interface slipping velocities.

1
2
3 **Appendix: DSC measurement on the phase transformation temperatures of**
4 **Ni-Mn-Ga Shape Memory Alloy**
5
6
7

8
9 To measure the four typical temperatures (M_s , M_f , A_s , and A_f) for the martensitic
10 transformation, the DSC test was performed on our material (Ni-Mn-Ga with the mass
11 48.2 mg) in a temperature range between 20°C and 120°C (by DSC Q20, SETARAM).
12
13 As the heating/cooling speed could influence these typical temperatures, three different
14 loading rates, 10 °C/min, 5 °C/min and 1 °C/min were utilized in the measurement
15
16 (1 °C/min is the minimum loading speed allowed in the machine). The obtained heat
17 flow curves at different loading rates are plotted in Fig. A1, from which the four typical
18 temperatures can be measured by the tangent method. The results are summarized in
19
20 the following Table A1. It is seen that the thermal hysteresis $T_{DSC}^H \equiv \frac{A_s + A_f - M_s - M_f}{2}$
21
22 decreases with decreasing loading rate. It should be noted that the rate dependence of
23 the measured hysteresis is mainly caused by the rate-dependent M_f and A_f . By contrast,
24
25 the measured values of M_s and A_s are not so sensitive to the loading rate.
26
27
28
29
30
31
32
33
34
35
36
37
38
39
40
41
42
43
44
45
46
47
48
49
50
51
52
53
54
55
56
57
58
59
60
61
62
63
64
65

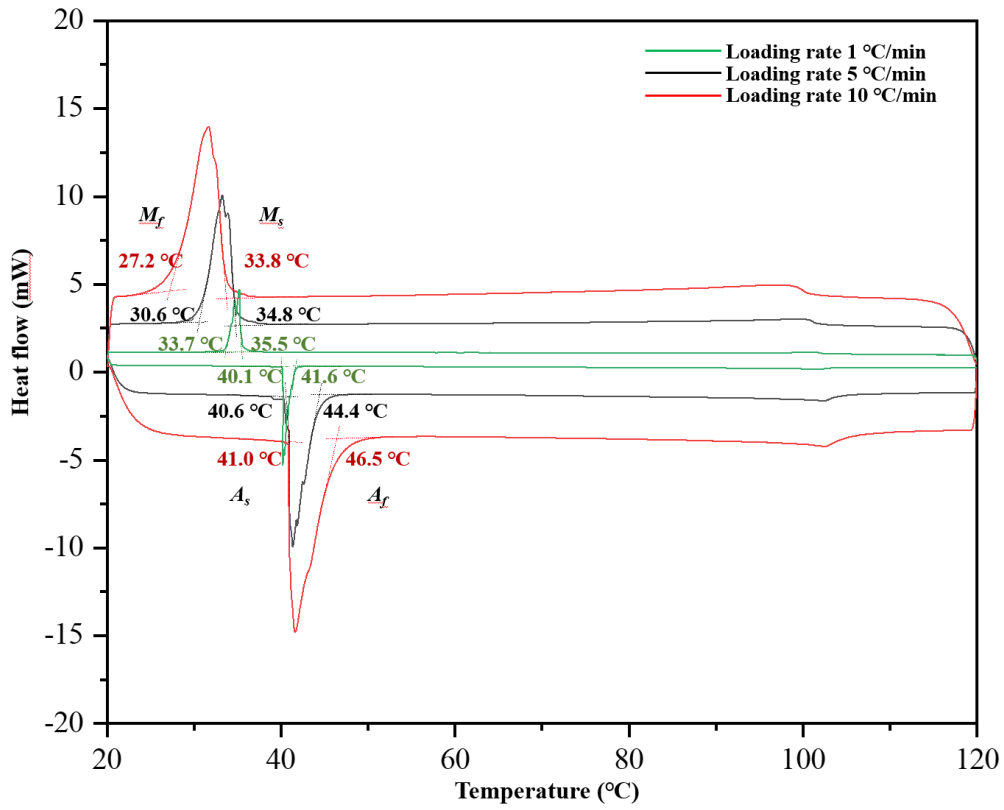


Fig. A1 DSC results of the Ni-Mn-Ga at different loading rates.

Table A1 The typical temperatures M_s , M_f , A_s , and A_f measured from Fig. A1.

| Loading rate (°C/min) | Transformation temperatures (°C) | | | | $T_{DSC}^H \equiv \frac{A_s + A_f - M_s - M_f}{2}$ (°C) |
|--------------------------|----------------------------------|-------|-------|-------|---|
| | M_s | M_f | A_s | A_f | |
| 1 | 35.5 | 33.7 | 40.1 | 41.6 | 6.3 |
| 5 | 34.8 | 30.6 | 40.6 | 44.4 | 9.8 |
| 10 | 33.8 | 27.2 | 41.0 | 46.5 | 13.3 |

Acknowledgements

Chengguan Zhang would like to acknowledge China Scholarship Council (CSC) for the financial support (NO. 202006890005).

Reference

- [1] Z. Zhang, R.D. James, S. Müller, Energy barriers and hysteresis in martensitic phase transformations, *Acta Mater.* 57(15) (2009) 4332-4352.
- [2] Y.J. He, Interface propagation and energy dissipation in Shape Memory Alloys, *Scripta Mater.* 230 (2023) 115420.
- [3] M. Sanati, R.C. Albers, T. Lookman, A. Saxena, First-order versus second-order phase transformation in AuZn, *Phys. Rev. B* 88(2) (2013) 024110.
- [4] M.A. Iadicola, J.A. Shaw, Rate and thermal sensitivities of unstable transformation behavior in a shape memory alloy, *Int. J. Plasticity* 20(4-5) (2004) 577-605.
- [5] J.A. Shaw, S. Kyriakides, On the nucleation and propagation of phase transformation fronts in a NiTi alloy, *Acta Mater.* 45(2) (1997) 683-700.
- [6] Y.J. He, H. Yin, R. Zhou, Q. Sun, Ambient effect on damping peak of NiTi shape memory alloy, *Mater. Lett.* 64(13) (2010) 1483-1486.
- [7] X. Liu, Q. Wang, S.Y. Kondrat'ev, P. Ji, F. Yin, C. Cui, G. Hao, Microstructural, mechanical, and damping properties of a Cu-based shape memory alloy refined by an in-situ LaB₆/Al inoculant, *Metallurgical Transactions A* 50 (2019) 2310-2321.
- [8] J. Mohd Jani, M. Leary, A. Subic, M.A. Gibson, A review of shape memory alloy research, applications and opportunities, *Materials & Design* 56 (2014) 1078-1113.
- [9] M. Grujcic, G.B. Olson, W.S. Owen, Mobility the β_1 - γ' martensitic interface in Cu-Al-Ni: Part I. Experimental measurements, *Metallurgical Transactions A* 16 (1985) 1723-1734.
- [10] Y.J. He, Q.P. Sun, On non-monotonic rate dependence of stress hysteresis of superelastic shape memory alloy bars, *Int. J. Solids struct.* 48(11-12) (2011) 1688-1695.

- 1 [11] H.E. Karaca, I. Karaman, B. Basaran, D.C. Lagoudas, Y.I. Chumlyakov, H.J. Maier, On the
2 stress-assisted magnetic-field-induced phase transformation in Ni₂MnGa ferromagnetic shape
3 memory alloys, *Acta Mater.* 55(13) (2007) 4253-4269.
4
5
6
7
8 [12] C. Zhang, G. Qin, S. Zhang, X. Chen, Y.J. He, Hysteresis effect on austenite-martensite
9 interface in Ni-Mn-Ga single crystal, *Scripta Mater.* 222 (2023) 115029.
10
11
12
13 [13] G. Qin, C. Zhang, S. Zhang, X. Chen, Y.J. He, Compatibility effect on stress-free two-way
14 memory of Ni-Mn-Ga single crystal, *J. Alloy Compd.* 935 (2023) 168134.
15
16
17
18 [14] R.J. Salzbrenner, M. Cohen, On the thermodynamics of thermoelastic martensitic
19 transformations, *Acta Metall.* 27(5) (1979) 739-748.
20
21
22
23 [15] J.M. Ball, K. Koumatos, H. Seiner, Nucleation of austenite in mechanically stabilized
24 martensite by localized heating, *J. Alloy Compd.* 577 (2013) S37-S42.
25
26
27
28 [16] M. Grujicic, G.B. Olson, Dynamics of martensitic interfaces, *Interface Science* 6 (1998) 155-
29 164.
30
31
32
33 [17] A. Amengual, F.C. Lovey, V. Torra, The hysteretic behaviour of a single-interface
34 martensitic transformation in Cu-Zn-Al Shape Memory Alloys, *Scripta Metallurgica et Materialia*
35 24 (1990) 2241-2246.
36
37
38
39 [18] M. Grujicic, G.B. Olson, W.S. Owen, Mobility of the β_1 - γ' martensitic interface in Cu-Al-Ni:
40 Part II. Model calculations, *Metallurgical Transactions A* 16(16) (1985) 1735-1744.
41
42
43
44 [19] Y. Tong, A. Shuitcev, Y. Zheng, Recent Development of TiNi-Based Shape Memory Alloys
45 with High Cycle Stability and High Transformation Temperature, *Advanced Engineering*
46 *Materials* 22(4) (2020) 1900496.
47
48
49
50 [20] D. Xue, R. Yuan, Y. Zhou, D. Xue, T. Lookman, G. Zhang, X. Ding, J. Sun, Design of High
51
52
53
54
55
56
57
58
59
60
61
62
63
64
65

1 Temperature Ti-Pd-Cr Shape Memory Alloys with Small Thermal Hysteresis, *Sci Rep* 6 (2016)
2
3 28244.

4
5
6 [21] R. Delville, S. Kasinathan, Z. Zhang, J.V. Humbeeck, R.D. James, D. Schryvers,
7
8
9 Transmission electron microscopy study of phase compatibility in low hysteresis shape memory
10
11 alloys, *Philosophical Magazine* 90(1-4) (2010) 177-195.

12
13
14 [22] R. Zarnetta, R. Takahashi, M.L. Young, A. Savan, Y. Furuya, S. Thienhaus, B. Maaß, M.
15
16
17 Rahim, J. Frenzel, H. Brunken, Y.S. Chu, V. Srivastava, R.D. James, I. Takeuchi, G. Eggeler,
18
19
20 A. Ludwig, Identification of Quaternary Shape Memory Alloys with Near-Zero Thermal
21
22 Hysteresis and Unprecedented Functional Stability, *Advanced Functional Materials* 20(12)
23
24 (2010) 1917-1923.

25
26
27 [23] J. Cui, Y.S. Chu, O.O. Famodu, Y. Furuya, J. Hattrick-Simpers, R.D. James, A. Ludwig, S.
28
29
30 Thienhaus, M. Wuttig, Z. Zhang, I. Takeuchi, Combinatorial search of thermoelastic shape-
31
32
33 memory alloys with extremely small hysteresis width, *Nat Mater* 5(4) (2006) 286-90.

34
35
36 [24] S. Zhang, X. Chen, Z. Moumni, Y.J. He, Thermal effects on high-frequency magnetic-field-
37
38
39 induced martensite reorientation in ferromagnetic shape memory alloys: An experimental and
40
41
42 theoretical investigation, *Int. J. Plasticity* 108 (2018) 1-20.

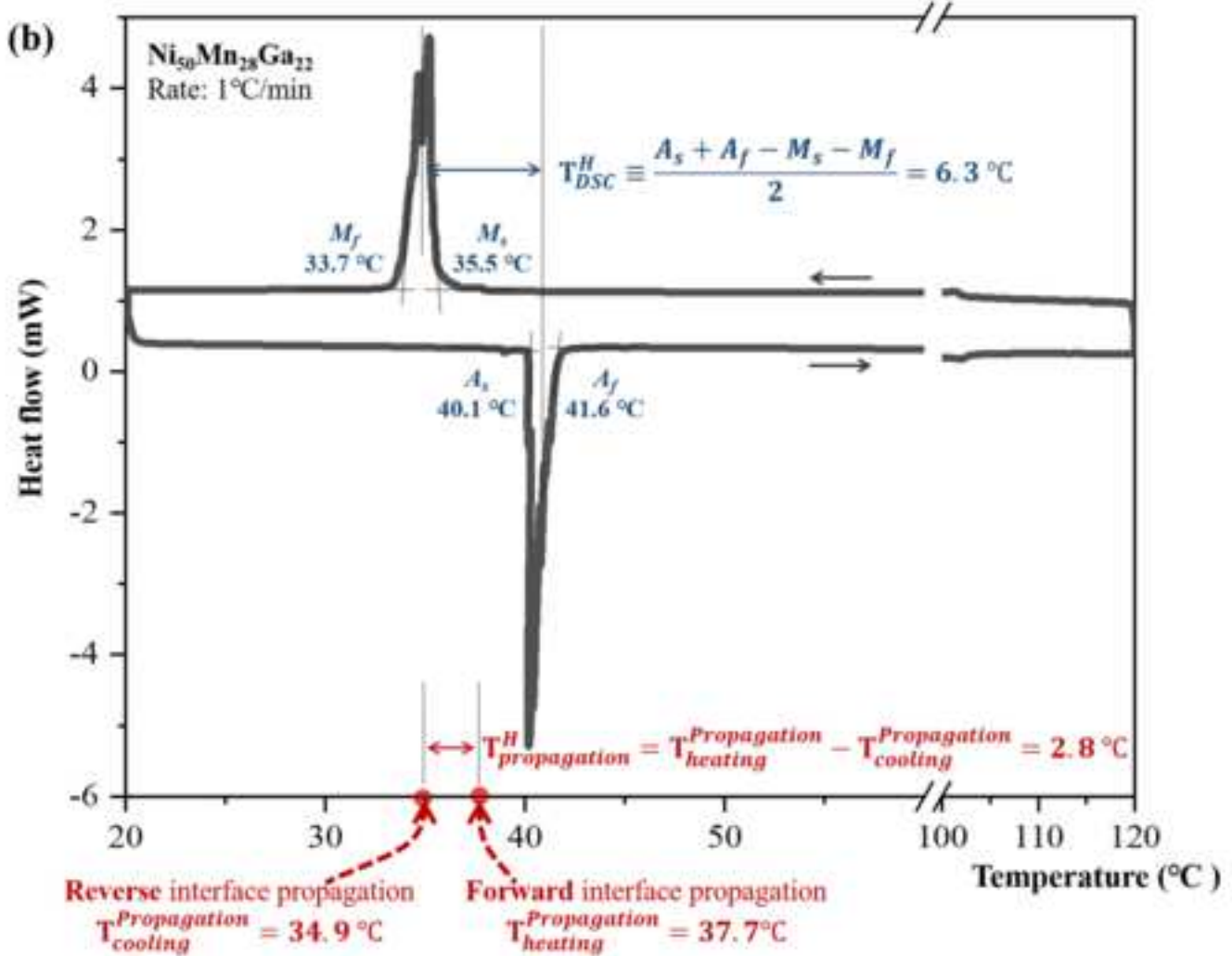
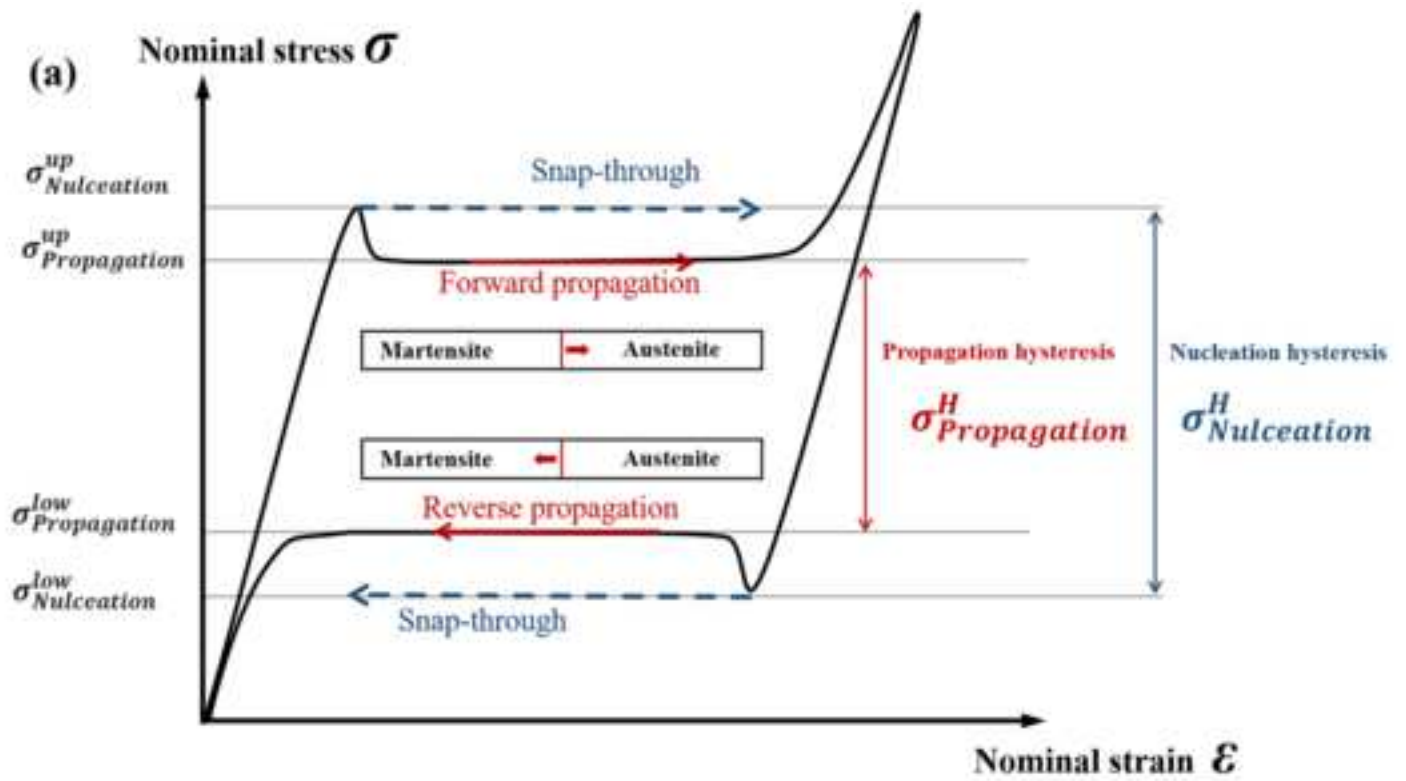
43
44
45 [25] S. Zhang, X. Chen, Z. Moumni, Y.J. He, Coexistence and compatibility of martensite
46
47
48 reorientation and phase transformation in high-frequency magnetic-field-induced deformation
49
50
51 of Ni-Mn-Ga single crystal, *Int. J. Plasticity* 110 (2018) 110-122.

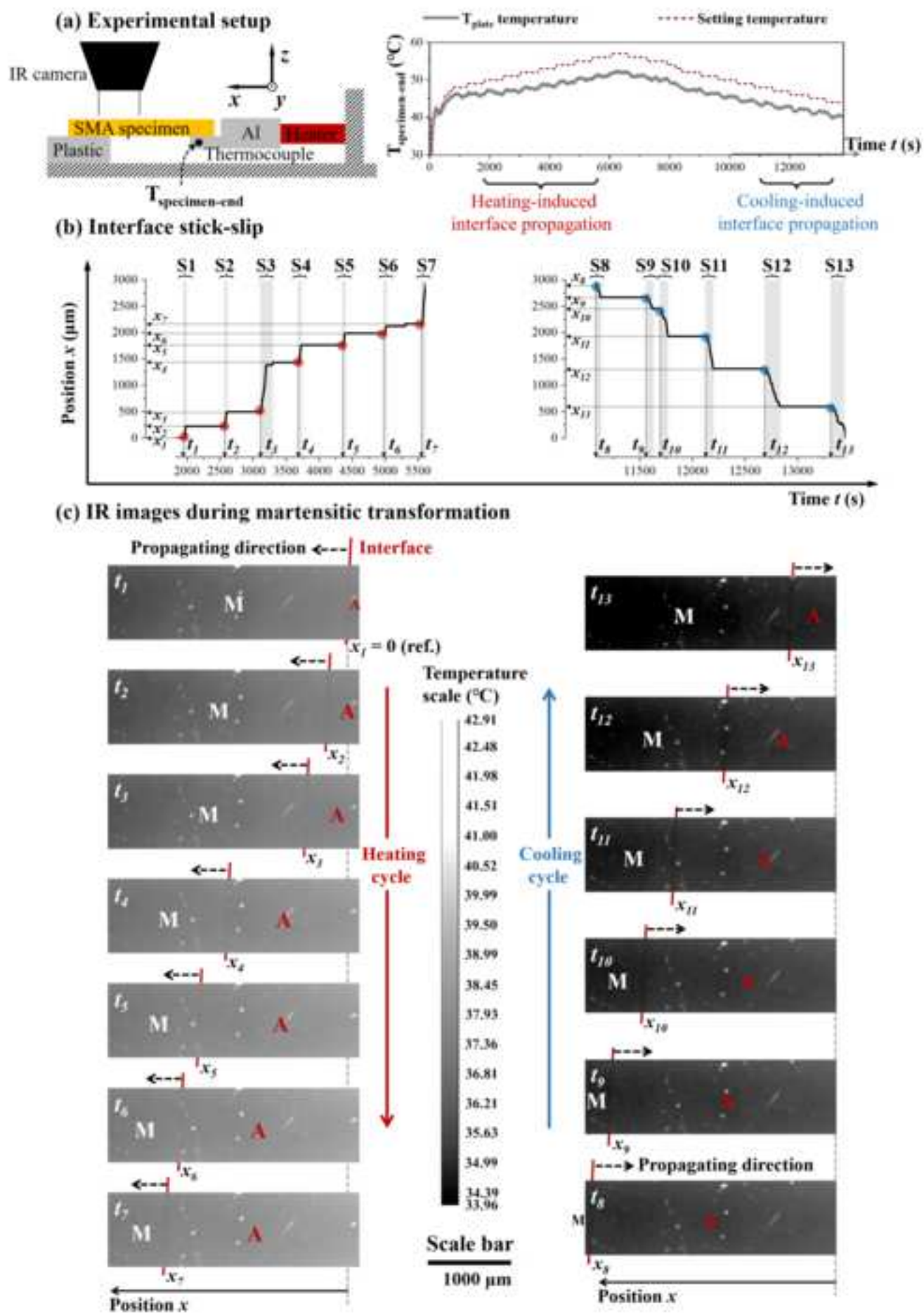
52
53 [26] L. Zheng, Y.J. He, Z. Moumni, Investigation on fatigue behaviors of NiTi polycrystalline
54
55
56 strips under stress-controlled tension via in-situ macro-band observation, *Int. J. Plasticity* 90
57
58
59 (2017) 116-145.

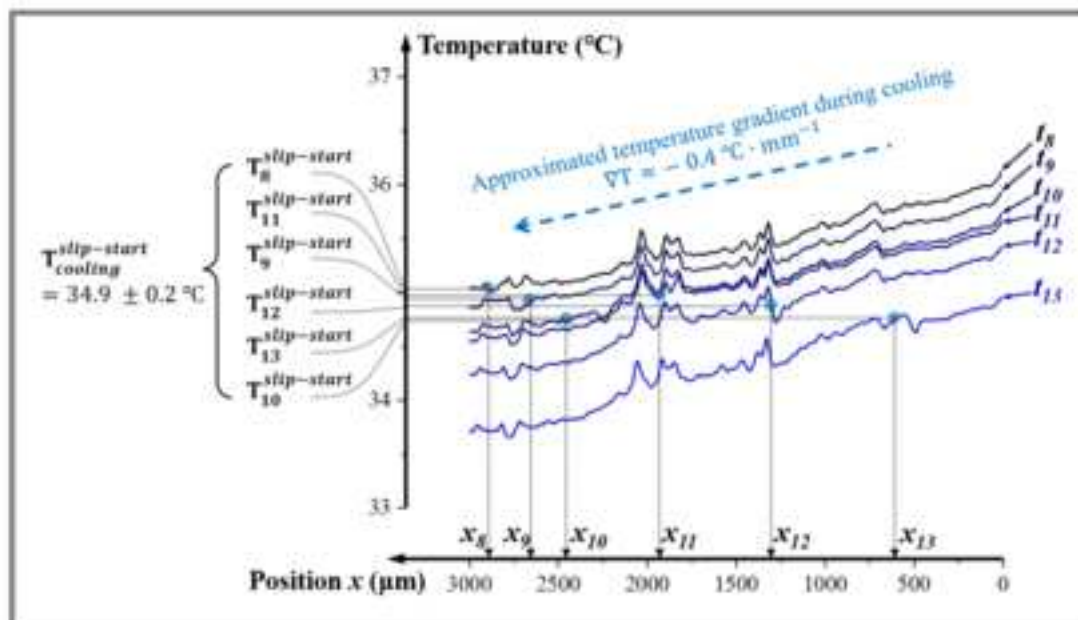
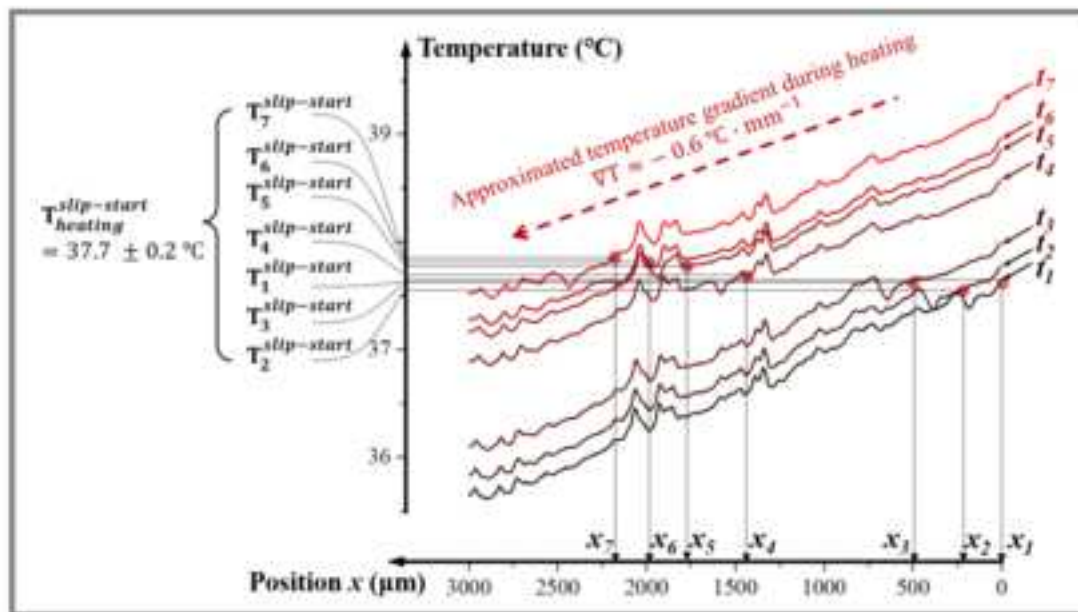
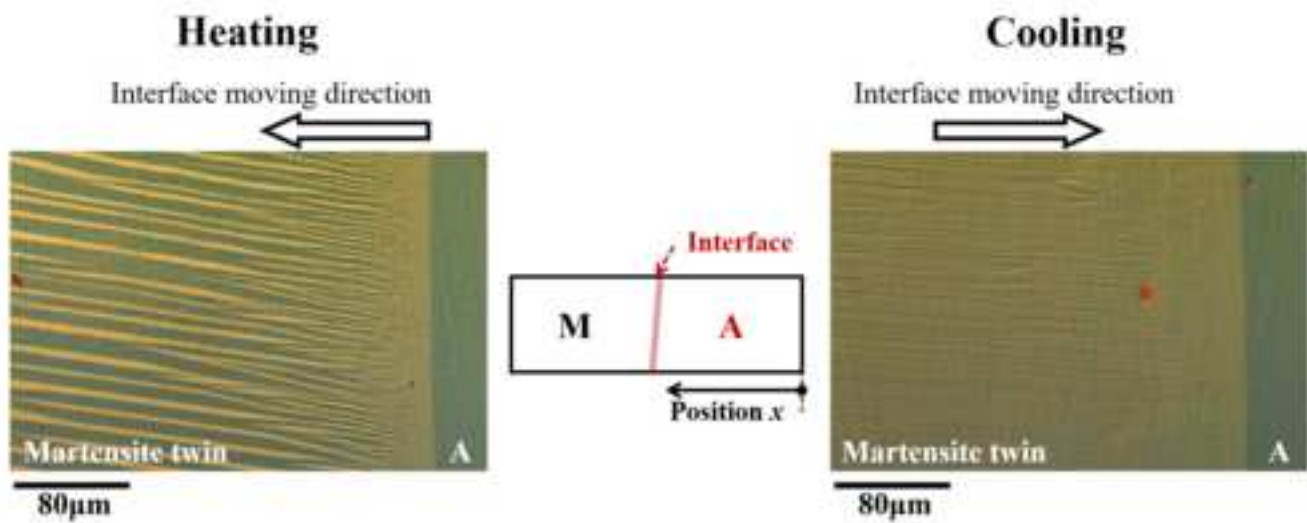
- 1 [27] H. Yin, M. Li, Q. Sun, Thermomechanical coupling in cyclic phase transition of shape
2
3 memory material under periodic stressing—experiment and modeling, *J. Mech. Phys. Solids*
4
5
6 149 (2021) 104199.
7
8
9 [28] E.A. Pieczyska, S.P. Gadaj, W.K. Nowacki, H. Tobushi, Phase-Transformation Fronts
10
11 Evolution for Stress- and Strain-Controlled Tension Tests in TiNi Shape Memory
12
13 Alloy, *Experimental Mechanics* 46(4) (2006) 531-542.
14
15
16 [29] H. Seiner, P. Plucinsky, V. Dabade, B. Benešová, R.D. James, Branching of twins in shape
17
18 memory alloys revisited, *J. Mech. Phys. Solids* 141 (2020) 103961.
19
20
21
22 [30] E. Bronstein, E. Faran, D. Shilo, Analysis of austenite-martensite phase boundary and
23
24 twinned microstructure in shape memory alloys: The role of twinning disconnections, *Acta Mater.*
25
26 164 (2019) 520-529.
27
28
29
30 [31] S. Stupkiewicz, G. Maciejewski, H. Petryk, Low-energy morphology of the interface layer
31
32 between austenite and twinned martensite, *Acta Mater.* 55(18) (2007) 6292-6306.
33
34
35
36 [32] K. Haldar, D.C. Lagoudas, I. Karaman, Magnetic field-induced martensitic phase
37
38 transformation in magnetic shape memory alloys: Modeling and experiments, *J. Mech. Phys.*
39
40 *Solids* 69 (2014) 33-66.
41
42
43
44 [33] X. Chen, Y.J. He, Thermo-magneto-mechanical coupling dynamics of magnetic shape
45
46 memory alloys, *Int. J. Plasticity* 129 (2020) 102686.
47
48
49
50 [34] Y. Song, X. Chen, V. Dabade, T.W. Shield, R.D. James, Enhanced reversibility and
51
52 unusual microstructure of a phase-transforming material, *Nature* 502(7469) (2013) 85-8.
53
54
55
56 [35] H. Shi, R. Delville, V. Srivastava, R.D. James, D. Schryvers, Microstructural dependence
57
58 on middle eigenvalue in Ti–Ni–Au, *J. Alloy Compd.* 582 (2014) 703-707.
59
60

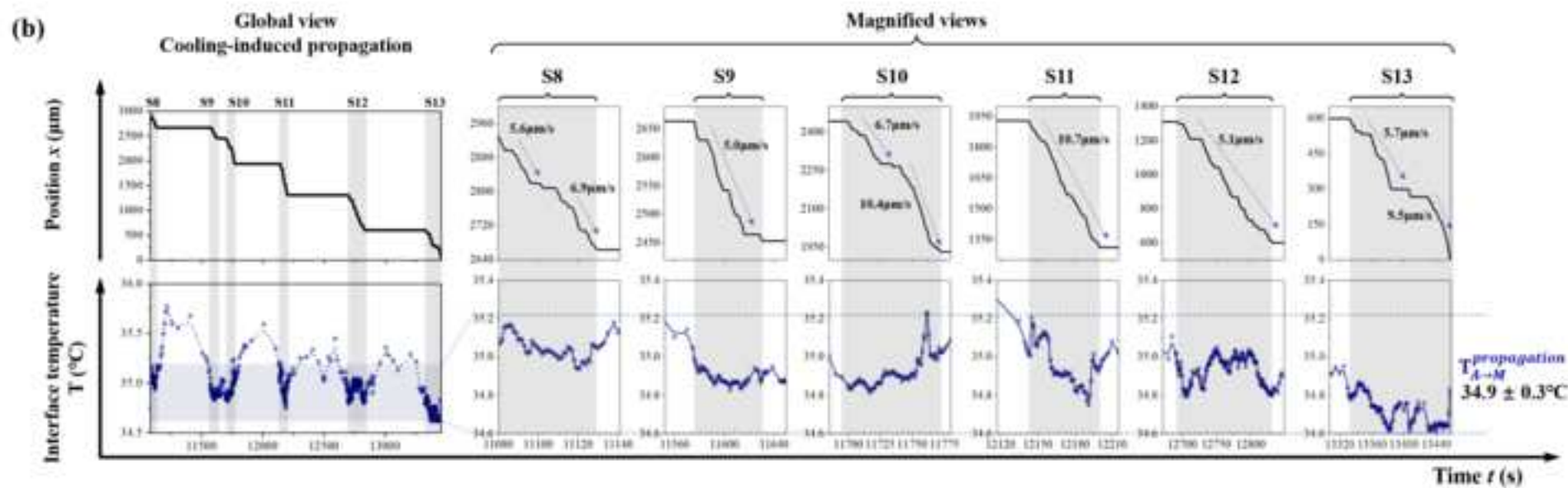
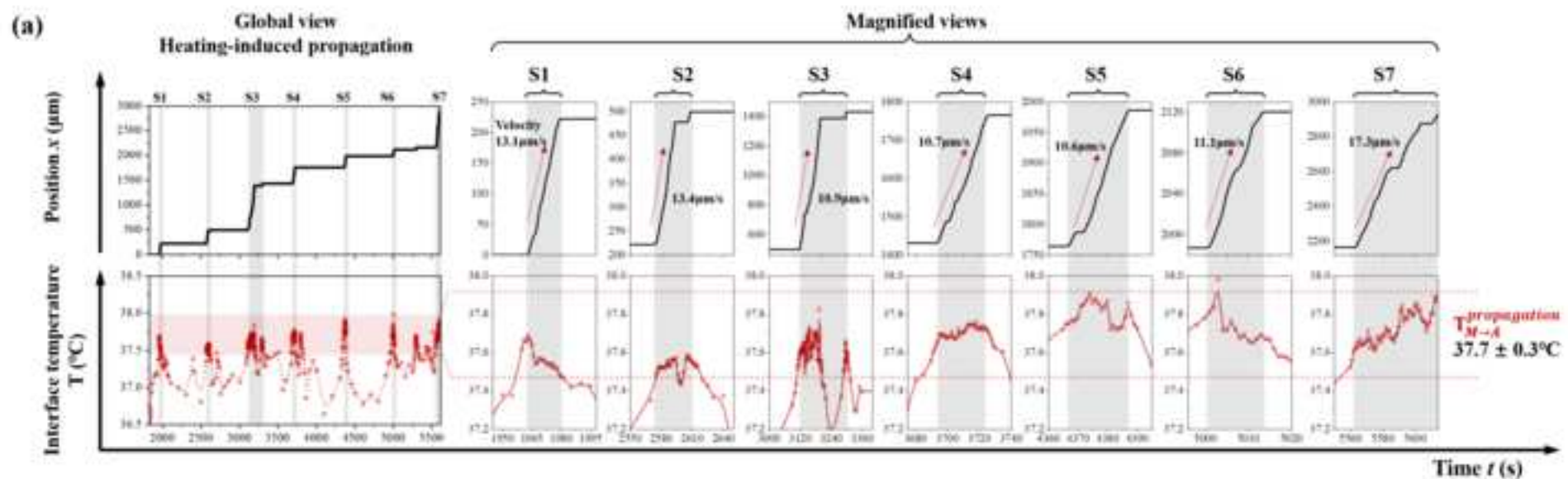
- 1 [36] C. Zhang, X. Balandraud, Y.J. He, Coexistence of five domains at single propagating
2 interface in single-crystal Ni-Mn-Ga Shape Memory Alloy, *J. Mech. Phys. Solids* 183 (2024)
3
4 105481.
5
6
7
8 [37] H. Petryk, S. Stupkiewicz, Interfacial energy and dissipation in martensitic phase
9 transformations. Part I: Theory, *J. Mech. Phys. Solids* 58(3) (2010) 390-408.
10
11
12 [38] W.-H. Wang, J.-L. Chen, Z.-h. Liu, G.-H. Wu, W.-S. Zhan, Thermal hysteresis and friction
13 of phase boundary motion in ferromagnetic Ni₅₂Mn₂₃Ga₂₅ single crystals, *Phys. Rev. B* 65(1)
14 (2001) 012416.
15
16
17 [39] D. Xue, Z. Li, Y. Pan, G. Zhang, Low hysteresis and high cyclic stability in a
18 Ti₅₀Ni_{45.2}Cu₁Fe_{3.8} shape memory alloy, *J. Alloy Compd.* 955 (2023) 170188.
19
20
21 [40] C. Seguí, V.A. Chernenko, J. Pons, E. Cesari, V. Khovailo, T. Takagi, Low temperature-
22 induced intermartensitic phase transformations in Ni–Mn–Ga single crystal, *Acta Mater.* 53(1)
23 (2005) 111-120.
24
25
26 [41] V. Pinneker, M. Gueltig, A. Sozinov, M. Kohl, Single phase boundary actuation of a
27 ferromagnetic shape memory foil, *Acta Mater.* 64 (2014) 179-187.
28
29
30 [42] O. Heczko, N. Lanska, O. Soderberg, K. Ullakko, Temperature variation of structure and
31 magnetic properties of Ni–Mn–Ga magnetic shape memory alloys, *J. Magn. Magn. Mater.* 242-
32 245 (2002) 1446-1449.
33
34
35 [43] S. Zhang, G. Qin, Y.J. He, Ambient effects on the output strain of Ni–Mn–Ga single crystal
36 magnetic shape memory alloy, *J. Alloy Compd.* 835 (2020) 155159.
37
38
39 [44] R. Chulist, P. Czaja, T. Tokarski, M. Faryna, Martensite stabilisation in single crystalline
40 Ni-Mn-Ga and Ni-Mn-Sn magnetic shape memory alloys, *Mater. Lett.* 230 (2018) 266-269.
41
42
43
44
45
46
47
48
49
50
51
52
53
54
55
56
57
58
59
60
61
62
63
64
65

1 [45] N. Lanska, O. Söderberg, A. Sozinov, Y. Ge, K. Ullakko, V.K. Lindroos, Composition and
2
3 temperature dependence of the crystal structure of Ni–Mn–Ga alloys, J. Appl. Phys. 95(12)
4
5
6 (2004) 8074-8078.
7
8
9
10
11
12
13
14
15
16
17
18
19
20
21
22
23
24
25
26
27
28
29
30
31
32
33
34
35
36
37
38
39
40
41
42
43
44
45
46
47
48
49
50
51
52
53
54
55
56
57
58
59
60
61
62
63
64
65



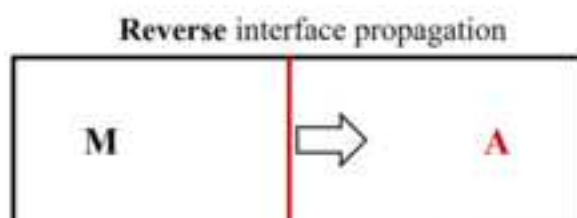




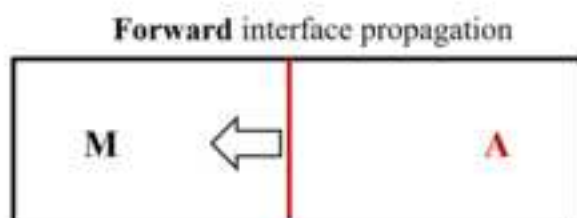


In-situ measurement on interface propagation

$$T_{propagation}^{ff} = T_{heating}^{Propagation} - T_{cooling}^{Propagation} = 2.8 \text{ } ^\circ\text{C}$$



$$T_{cooling}^{Propagation} = 34.9 \text{ } ^\circ\text{C}$$



$$T_{heating}^{Propagation} = 37.7 \text{ } ^\circ\text{C}$$

DSC measurement

$$T_{DSC}^H \equiv \frac{A_s + A_f - M_s - M_f}{2} = 6.3 \text{ } ^\circ\text{C}$$

